4

Multi-dimensional Imaging by Compressive Digital Holography

Yair Rivenson[1], Adrian Stern[2], Joseph Rosen[1], and Bahram Javidi[3]
[1]*Department of Electrical and Computer Engineering, Ben-Gurion University of the Negev, Israel*
[2]*Department of Electro-Optics Engineering, Ben-Gurion University of the Negev, Israel*
[3]*Department of Electrical and Computer Engineering, University of Connecticut, USA*

4.1 Introduction

Unlike standard imaging, digital holography allows an indirect way to capture the complex field amplitude of a wavefront originating from an object. This provides three-dimensional (3D) information on the object recorded in a single two-dimensional (2D) recording device. Currently, digital holography is captured using a semiconductor based device and often reconstructed using numerical means on a computer. This type of holography is referred to as *Digital Holography* (DH) [1]. Digital holography is used in many areas including 3D imaging, digital holographic microscopy, aberration correction, holographic interferometry, and object surface and tomographic imaging.

During the last few years, holography was successfully combined with the rapidly growing signal acquisition-reconstruction scheme known as compressive sensing (CS) [2–5]. With introduction of CS, a theory that introduced a dramatic breakthrough in signal acquisition, implementations in optics were pursued. Shortly, research groups working on the implementation of the CS principle in optics realized that holography is a natural field for applications of CS principles [6–11]. The synergy between holography and compressive sensing has yielded new applications and also addressed classical holographic problems. Many compressive digital holographic sensing applications were demonstrated using different optical setups and having different goals. Amongst them are compressive Gabor holography [8], compressive Fresnel holography [9,11], off-axis frequency shifting holography [10], millimeter wave compressive holography [12], off-axis holography of diffuse objects [13], sectioning from optical scanning

Multi-dimensional Imaging, First Edition. Edited by Bahram Javidi, Enrique Tajahuerce and Pedro Andrés.

holography [14], super-resolved wide field florescent microscopic holography [15,16], recovery of an object from holography in low illumination conditions [17], reduced scanning effort in incoherent multiple view-projection holography [18], video rate microscopic tomography [19], the use of compressive holography to see through partially occluding objects [20], single shot acquisition of spatial, spectral, and polarimetric information using a single exposure acquired hologram [21], nanometer accuracy object localization [22] and improved tomographic object reconstruction with multiple illumination angles [23,24]. The works in [25,26] provide an overview of the subject. The growing number of publications in the field indicates the importance of an obvious indication for the importance of the field.

This chapter reviews both the theoretical and the applicative aspects for using compressive sensing in digital holography. First, we equip the reader with the relevant background on compressive sensing. We then show how compressive sensing can be applied to DH, where the presentation is divided into three main parts, corresponding to different DH aspects that benefit from the CS theory:

1. Sensor design, particularly reducing the number of detector pixels, or baseline projections.
2. Reconstruction of an object from its truncated wavefront after encountering partially opaque obstacles.
3. Reconstruction of 3D object tomography from a single 2D projection.

4.2 Compressive Sensing Preliminaries

This section surveys briefly the theory of compressive sensing [2,3]. CS theory asserts that one can recover sparse signals and images from far fewer samples or measurements than traditional methods. Sparsity expresses the idea that the "information rate" of a continuous signal may be much smaller than its bandwidth, or in other words, that a discrete signal depends on a number of degrees of freedom that is much smaller than its (finite) length. More precisely, compressive sampling exploits the fact that many natural signals are sparse or compressible in the sense that they have concise representations when expressed in the proper basis or dictionary, $\mathbf{\Psi}$. The sparsifying transform $\mathbf{\Psi}$ may be the Fourier or some wavelet basis, or a dictionary of waveforms tailored from *a-priori* information about the object.

The sensing mechanism requires correlating the signal with a small number of fixed waveforms that are incoherent (in the sense defined in Section 4.2.1) with the sparsifying basis $\mathbf{\Psi}$. Signal reconstruction is performed numerically using appropriate algorithms. A block diagram of the CS process is shown in Fig. 4.1.

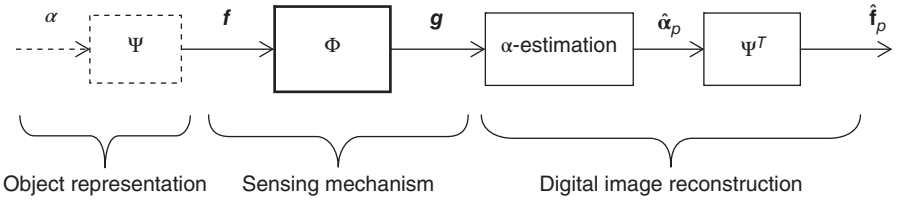

Figure 4.1 Imaging scheme of compressed sensing [27]. *Source*: A. Stern and B. Javidi 2007. Reproduced with permission from The Optical Society

The signal\image $\boldsymbol{f}$ consisting of N samples\pixels is sensed by taking a set, $\boldsymbol{g}$, of M projections. We assume that $\boldsymbol{f}$ has a sparse representation in some known domain so that it can be composed by a transform $\boldsymbol{\Psi}$ and only S nonzero coefficients of a vector $\boldsymbol{\alpha}$, that is, $\boldsymbol{f} = \boldsymbol{\Psi\alpha}$, where only S ($S \ll N$) entries of $\boldsymbol{\alpha}$ are nonzero. We refer to such an object as an S-sparse object. The transform $\boldsymbol{\Psi}$ can be for instance the Fourier or wavelet transforms that are commonly used in digital compression techniques. The sensing step is represented by the operator $\boldsymbol{\Phi}$ in Fig. 4.1. Mathematically, $\boldsymbol{\Phi}$ can be represented by an M by N matrix, hence the ith component of the measurement vector $\boldsymbol{g}$ is given by:

$$g_j = \langle f, \phi_i \rangle, \qquad i = 1, 2, \ldots M, \tag{4.1}$$

where ϕ_i is the ith row of $\boldsymbol{\Phi}$, and $\langle \cdot, \cdot \rangle$ denotes the inner product. That is, we simply correlate the object we wish to acquire with the waveforms ϕ_i. For instance, if the sensing waveforms are Dirac deltas ("spikes"), then $\mathbf{g}$ is a vector of sampled values of $\boldsymbol{f}$ in the time or space domain. Particularly, if the sensing waveforms are indicator functions of pixels, then $\boldsymbol{g}$ is the image collected by sensors in an ideal digital camera. CS applies in the case that $M < N$, meaning that the sensed signal is undersampled in the conventional sense. This means that there are more variables than equations leading to an underdetermined system of equations. The reconstruction of $\boldsymbol{f}$ from the measurement $\boldsymbol{g}$ is a highly ill-posed problem. A classic approach for such data inversion would be to minimize the root mean square error between $\boldsymbol{\alpha}$ and the estimated solution $\widehat{\boldsymbol{\alpha}}$:

$$\widehat{\boldsymbol{\alpha}} = \min \|\boldsymbol{\alpha}\|_2 \ \textit{such that}\ \mathbf{g} = \boldsymbol{\Omega\alpha}, \tag{4.2}$$

where $\boldsymbol{\Omega}_{M\times N} = \boldsymbol{\Phi\Psi}$, is the operator combining the sensing and sparsity operators. This solution, however, does not take advantage of the sparsity of the image and therefore does not necessarily lead to the correct reconstruction. Given the *a-priori* information that the signal can be sparsely represented, an intuitively more appropriate approach would be to apply the ℓ_0-norm solution that satisfies the given constraints. Thus, $\widehat{\boldsymbol{\alpha}}$ is defined as:

$$\widehat{\boldsymbol{\alpha}} = \min \|\boldsymbol{\alpha}\|_0 \ \textit{such that}\ \mathbf{g} = \boldsymbol{\Omega\alpha}, \tag{4.3}$$

where $\|\boldsymbol{\alpha}\|_p = \left(\sum_{i=1}^{N} |\boldsymbol{\alpha}_i| \right)^{1/p}$ is the ℓ_p norm of $\boldsymbol{\alpha}$. The ℓ_0-norm solution program (4.3) simply counts the number of nonzero terms in all possible $\boldsymbol{\alpha}$ (that satisfy the acquisition model, $\mathbf{g} = \boldsymbol{\Omega\alpha}$) and chooses the one with the fewest number of terms. Unfortunately, solving this problem essentially requires exhaustive searches over all subsets of columns of $\boldsymbol{\Omega}$, a procedure which is combinatorial in nature and has exponential complexity. This computational intractability has led researchers to develop alternatives to the ℓ_0-norm solution [2,3,28]. One of the approaches (frequently used in CS theory) is the minimum ℓ_1-norm solution according to which $\widehat{\boldsymbol{\alpha}}$ is found by:

$$\widehat{\boldsymbol{\alpha}} = \min \|\boldsymbol{\alpha}\|_1 \ \textit{such that}\ \mathbf{g} = \boldsymbol{\Omega\alpha}. \tag{4.4}$$

Unlike the ℓ_0-norm, which counts the nonzero coordinates, the ℓ_1-norm is convex and thus can be recast as linear programming. A linear program is solved in polynomial time, while the ℓ_0-norm is solved in combinatorial time. In many cases, the minimum ℓ_1-norm solution is a good approximation of the minimum ℓ_0-norm solution [2,4,28,29].

Another minimization problem, which is often used in the context of compressive sensing, is formulated using total variation (TV) minimization [30] as follows:

$$\min_f TV(f) \quad such\ \ that \quad \mathbf{g} = \mathbf{\Phi f}$$

$$\text{with } TV(f) = \sqrt{(f_{i+1,j} - f_{i,j})^2 + (f_{i,j+1} - f_{i,j})^2}. \tag{4.5}$$

This framework is extensively being used in compressive imaging applications, and only recently its performance guarantees were formulated [31].

The uniqueness of the solution of Eq. (4.4) and the equivalence between the ℓ_1 norm and the ℓ_0 norm solution holds if the number of compressive measurements M obeys certain conditions. These conditions can be derived from the signal sparsity and the coherence between the sensing and sparsifying operators and quantified using the *coherence parameter*. The coherence parameter expresses the idea that objects having a sparse representation in $\mathbf{\Psi}$ must be spread out, in the domain in which they are sensed, just as a spike in the time domain is spread out in the frequency domain. We shall distinguish between two different definitions of the coherence parameter, each applicable for different sensing system schemes.

4.2.1 The Coherence Parameter

4.2.1.1 Compressive Sensing by Uniformly Random Subsampling

In this measurement scheme we uniformly place our detectors at random in our measurement plane [4,29]. Mathematically, it is described as uniformly picking M out of N rows of $\mathbf{\Phi}$ at random, where $\mathbf{\Phi}$ is an $N \times N$ matrix describing the optical sensing operator in nominal sampling conditions. In this case, the appropriate coherence parameter definition is:

$$\mu_1 = \max_{i,j} |\langle \phi_i, \psi_j \rangle|, \tag{4.6}$$

where $\boldsymbol{\phi}_i$ is a row vector of $\mathbf{\Phi}$, $\boldsymbol{\psi}_j$ is a column vector of $\mathbf{\Psi}$, and $\langle \cdot, \cdot \rangle$ denotes inner product. Thus, μ_1 measures the incoherence, or dissimilarity, between sensing and sparsifying operators. In the common case that $\mathbf{\Phi}$ and $\mathbf{\Psi}$ are orthonormal bases it can be shown that $1/\sqrt{N} \leq \mu_1 \leq 1$ [4,29]. According to the CS theory the signal can be reconstructed by taking M uniformly at random projections obeying [4,29]:

$$\frac{M}{N} \geq C \mu_1^2 S \log N, \tag{4.7}$$

where C is a small constant. It is clear from Eq. (4.7) that the smaller μ_1 is, the smaller the relative number of measurements required to allow for accurate reconstruction of the signal. The uniformly at random sampling scheme is useful when reducing the sensing effort is desired. For example, this may be the case when only a relatively small number of detectors are allowed due to the substantial cost of each detector.

4.2.1.2 Compressive Sensing by Structured Subsampling

This sampling scheme refers to the case when we cannot idealize (in the CS sense) the subsampling mechanism to be randomly uniform or that the sensing operator cannot be considered as

an orthonormal basis (prior to its subsampling). In this case, the coherence parameter should be calculated as follows [5]:

$$\mu_2 = \max_{i \neq j} \frac{|\langle \omega_i, \omega_j \rangle|}{\|\omega_i\|_2 \|\omega_j\|_2}, \tag{4.8}$$

where $\langle \cdot, \cdot \rangle$ denotes inner product, ω_i is the column vector of $\mathbf{\Omega} = \mathbf{\Phi\Psi}$, $\Omega \in \mathbb{C}^{M \times N}$, and $\|.\|_2$ is the ℓ_2-norm. It can be shown that $\sqrt{(N-M)/[M(N-1)]} \leq \mu_2 \leq 1$. Using this definition, an S-sparse signal reconstruction guarantee is given by [5]:

$$S \leq \frac{1}{2}\left\{1 + \frac{1}{\mu_2}\right\}. \tag{4.9}$$

As μ_2 gets smaller we can accurately reconstruct higher dimensional S-sparse signals. As the number of measurements $M \to N$, the coherence parameter $\mu_2 \to 0$, for large M. The structured subsampling case is more suitable for describing sensing mechanisms where we wish to extract more information from a measurement where its subsampling mechanism is imposed by the physical attributes of a given system, as we shall see in the rest of the chapter.

4.3 Conditions for Accurate Reconstruction of Compressive Digital Holographic Sensing

4.3.1 Compressive Sensing Reconstruction Performance for a Plane Wave Illuminated Object

In this subsection we discuss reconstruction of an object where the measurement is given by its Fresnel transform. Let us consider the 2D free-space propagation conditions in the Fresnel approximation. The input object, $f(x,y)$, is illuminated by a plane wave of wavelength λ and the complex values of a propagating wave are measured at a plane which lies at distance z away from the input plane (as illustrated in Fig. 4.2) such that:

$$\begin{aligned} g(x,y) &= f(x,y) * \exp\left\{\frac{j\pi}{\lambda z}\left(x^2+y^2\right)\right\} \\ &= \exp\left\{\frac{j\pi}{\lambda z}\left(x^2+y^2\right)\right\} \iint f(\xi,\eta) \exp\left\{\frac{j\pi}{\lambda z}\left(\xi^2+\eta^2\right)\right\} \exp\left\{\frac{-j2\pi}{\lambda z}(x\xi+y\eta)\right\} d\xi d\eta. \end{aligned} \tag{4.10}$$

where "*" denotes convolution in Eq. (4.10). In order to capture $g(x,y)$ any of the well-known digital holographic recording techniques can be used [1]. The quadratic phase term

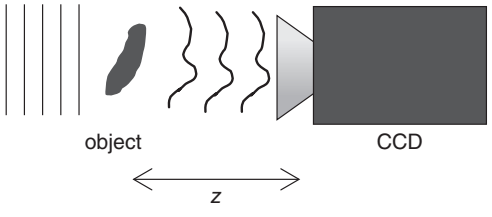

Figure 4.2 Fresnel propagation from an object illuminated by a plane wave [26]. *Source*: Y. Rivenson, A. Stern, and B. Javidi 2013. Reproduced with permission from The Optical Society

$\exp\{j\pi(x^2+y^2)/(\lambda z)\}$ determines the behavior of the Fresnel integral. In the Fraunhofer approximation regime as $\lambda z \to \infty$, the Fresnel transform approaches the Fourier transform. Fourier transform is extensively used in CS literature as a preferred sensing operator [4,29,32] because it holds low coherence with the canonical (unit) and several wavelet expansions [33]. This provides the main motivation for applying CS in DH. However, as $\lambda z \to 0$ the captured field approaches the object's field distribution. In such a case, the coherence parameter between the object and hologram plane receives its maximal value, meaning that the compressive sensing ratio $M/N \to 1$; that is, the number of measurements needs to be exactly the same as the number of pixels representing the object. Thus, we see that the Fresnel sensing basis is dependent on the reconstruction distance z and the wavelength λ, therefore, the performance of compressive digital holographic sensing depends on these parameters as well.

In order to analyze the dependence of compressive digital holographic sensing on z and other optical system parameters, we need to also account for the fact that in DH the numerical version of the Fresnel wave propagation (Eq. 4.10) is used. To do so, we need to distinguish between *near* and *far* field numerical approximations [34]. The numerical near field approximation is given by:

$$g(p\Delta x_o, q\Delta x_o) = \mathcal{F}_{2D}^{-1} \exp\left\{-j\pi\lambda z\left(\frac{m^2}{N\Delta x_0^2}+\frac{n^2}{N\Delta y_0^2}\right)\right\}\mathcal{F}_{2D}\{f(l\Delta x_0, k\Delta y_0)\}, \tag{4.11}$$

where Δx_0, Δy_0 are object and CCD resolution pixel size, with $0 \le p,q,k,l \le \sqrt{N}-1$ and $\mathcal{F}_{2D}$ is the 2D Fourier transform. We assume that the size of the object and sensor size are $\sqrt{N}\Delta x_0 \times \sqrt{N}\Delta y_0$. The near field model is valid for the regime where $z \le z_0 = \sqrt{N}\Delta x_0^2/\lambda$ [34]. For the working regime of $z \ge z_0 = \sqrt{N}\Delta x_0^2/\lambda$ the far field numerical approximation is given by the following:

$$\begin{aligned} &g(p\Delta x_z, q\Delta y_z) \\ &= \exp\left\{\frac{j\pi}{\lambda z}\left(p^2\Delta x_z^2 + q^2\Delta y_z^2\right)\right\}\mathcal{F}_{2D}\left[f\left(k\Delta x_0, l\Delta y_0\right)\exp\left\{\frac{j\pi}{\lambda z}\left(k^2\Delta x_0^2 + l^2\Delta y_0^2\right)\right\}\right], \end{aligned} \tag{4.12}$$

where $\Delta x_z = \lambda z/(\sqrt{N}\Delta x_0)$ is the output field's pixel size.

Let us consider the case where one wishes to design a sensing system that samples the object's diffraction field at some distance away from it using a small number of detectors. In this case the sensing system is best described using the randomly uniform subsampling scheme. If the object is sparse in the spatial domain, that is, $\Psi = \mathbf{I}$, it is shown in [11] that the coherence parameter for the near field numerical approximation is given by:

$$\mu_{1(near\ \ field)} = N[\Delta x_0^2/(\lambda z)]^2, \tag{4.13}$$

which means that the number of compressive measurements that are needed to accurately reconstruct the object is given by:

$$M \ge CN_F^2\frac{S}{N}\log N, \tag{4.14}$$

where N_F denotes the recording device Fresnel number $N_F = N\frac{\Delta x_0 \Delta y_0}{4\lambda z}$ and C is a small constant factor [29]. Equation (4.14) determines that as the working distance gets larger, N_F decreases

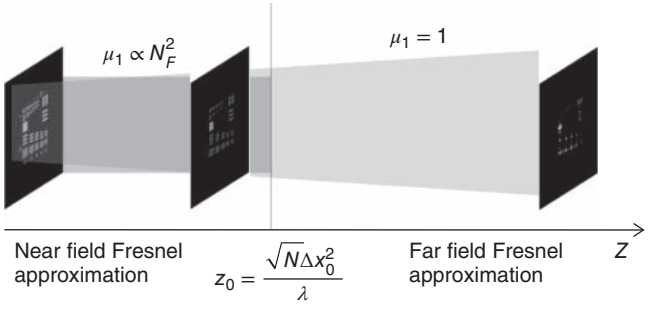

Figure 4.3 Illustration of numerical near and far field diffraction, and its relation with the coherence parameter, μ_1[26], *Source*: Y. Rivenson, A. Stern, and B. Javidi 2013. Reproduced with permission from The Optical Society

implying that fewer samples are required in order to reconstruct the signal accurately. It can be shown (see [11]) that when the near field approximation is not valid, the far field numerical approximation can be considered, and the coherence parameter becomes:

$$\mu_{1_{(near\ field)}} = 1. \tag{4.15}$$

The number of required measurements is given by:

$$M \geq CS \log N, \tag{4.16}$$

which remains constant regardless of working distance. A physical intuition about these results is illustrated in Fig. 4.3 and explained as follows: It is known that the object's diffraction pattern spatial spread is inversely proportional to its Fresnel number. Thus, as we move away from the object plane (and the Fresnel number decreases) each sample contains information about a larger portion of the object. This implies that discarding some of the samples is possible since the missing information can be extracted from other samples, thus allowing reduction in the number of samples required to accurately reconstruct the object.

4.3.2 Compressive Sensing Reconstruction Performance for a Spherical Wave Illuminated Object

In many holographic applications, the object is illuminated by a spherical wavefront, especially in compact microcopy (lensless) systems. This illumination scheme is illustrated in Fig. 4.4.

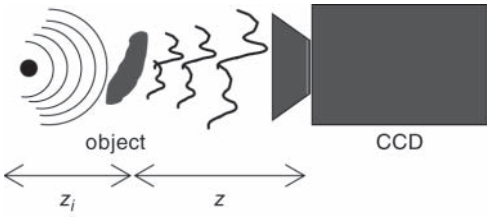

Figure 4.4 Fresnel propagation from an object illuminated by a diverging spherical wave

In this case, the calculation of the coherence parameter is slightly changed. Fresnel approximation for a 1D (for simplicity) diverging spherical wave in the free space is given by:

$$g(x) = \exp\left(j\pi\frac{x^2}{\lambda z_i}\right) f(x,y) * \exp\left(j\pi\frac{x^2}{\lambda z}\right) = \int \exp\left(j\pi\frac{\xi^2}{\lambda z_i}\right) f(\xi,\eta)\exp\left(j\pi\frac{(x-\xi)^2}{\lambda z}\right) d\xi$$
$$= \exp\left(j\pi\frac{x^2}{\lambda z}\right)\int f(\xi)\exp\left(j\pi\frac{\xi^2}{\lambda}\left(\frac{1}{z}+\frac{1}{z_i}\right)\right)\exp\left\{\frac{-j2\pi}{\lambda z}(x\xi)\right\} d\xi. \tag{4.17}$$

For proper numerical representation, one can follow the same trail that leads to the determination of the near and far field numerical approximations for the plane wave case. Accordingly, the sampling criterion for the far field model is given by [34]:

$$\frac{\Delta x_0^2}{\lambda}\left(\frac{1}{z}+\frac{1}{z_i}\right) < \frac{1}{\sqrt{N}}, \tag{4.18}$$

from which we can derive the far field limit of the Fresnel transform:

$$z > z_0 = \frac{\sqrt{N}\Delta x_0^2}{\lambda - \sqrt{N}\Delta x_0^2/z_i}. \tag{4.19}$$

It is evident that the far field limit is dependent on the distance between the illumination source and the object and is higher compared with the plane wave case due to the $-\sqrt{N}\Delta x_0^2/z_1$ term in the denominator. Therefore, we can rewrite the coherence parameter, for the near field Fresnel approximation, when a spherical illumination is used as:

$$\mu_1 = \frac{\sqrt{N}\Delta x_0^2}{z(\lambda - \sqrt{N}\Delta x_0^2/z_i)}. \tag{4.20}$$

As in the previous case, in the far field approximation $\mu_1 = 1$. In the limit of $\lambda z_i \to \infty$, Eq. (4.20) reduces to the coherence parameter, μ_1, for the case of planar field illumination:

$$\mu_1(\lambda z_i \to \infty) = \sqrt{N}\Delta x_0^2/(\lambda z) = \mu_{1(\textit{plane wave})}. \tag{4.21}$$

Equation (4.21) shows us that the coherence factor obtained with the diverging spherical wave is higher than that with plane wave. Hence, the number of required samples with spherical wave illumination is higher. For the 2D case, it can be shown that [35]:

$$\mu^{2D} = \sqrt{N}\frac{\Delta x_0^2}{z(\lambda - \sqrt{N}\Delta x_0^2/z_i)}\sqrt{N}\frac{\Delta y_0^2}{z(\lambda - \sqrt{N}\Delta y_0^2/z_i)}, \tag{4.22}$$

therefore, the required number of samples in the near field regime for the case where $\Delta x_0 = \Delta y_0$ is given by:

$$M \geq CN\left(\frac{\Delta x_0^2}{z_2\left(\lambda - \sqrt{N}\Delta x_0^2/z_1\right)}\right)^2 S\log N. \tag{4.23}$$

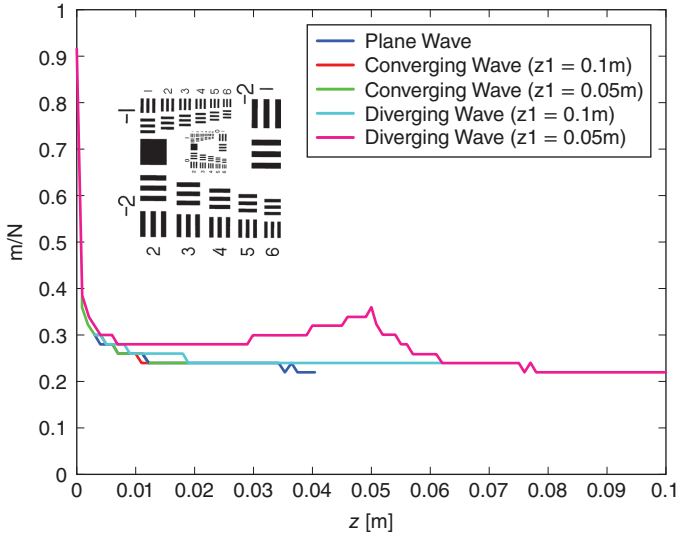

Figure 4.5 Compressive sensing ratio dependence on z for planar and spherical wave illumination. Simulation results obtained for the USAF 1951 resolution chart (*inset*)

Note that an illumination with a converging plane wave will give the opposite result, that is, the coherence parameter would be smaller for the same z distance of the object from the detector. The coherence parameter for the 1D converging wave is given by:

$$\mu_1 = \frac{\sqrt{N}\Delta x_0^2}{z(\lambda + \sqrt{N}\Delta x_0^2/z_i)}, \tag{4.24}$$

which means that for some applications it might be beneficial to use the converging wave illumination when the system number of pixels is the main issue rather than its axial compactness.

Figure 4.5 shows the compressive measurement ratio M/N as a function of imaging distance for different illumination schemes (planar wave, converging wave, and diverging wave). The results were obtained by simulating a compressive sensing Fresnel holography with undersampling the hologram field. The object used was a 1024×1024 pixel 1951 USAF resolution chart. The pixel spacing of the resolution chart is $\Delta x_0 = 5$ μm and the illuminating wavelength was $\lambda = 632.8$ nm. The detector was assumed to have 1024×1024 pixels. Fresnel samples were randomly chosen for different values of z. The algorithm ceased whenever it reached 32 dB reconstruction PSNR. From Fig. 4.5, it is evident that the compressive measurement ratio M/N was worse for the diverging wave illumination than for plane wave illumination. In this example converging wave illumination does not show any significant advantage over the planar wave illumination.

4.3.3 Reconstruction Performance for Non-Canonical Sparsifying Operators

When the object is not sparse in the spatial domain, that is, the sparsifying operator $\Psi \neq \mathbf{I}$, the number of necessary measurements, M, may differ according to the coherence parameter, μ_1,

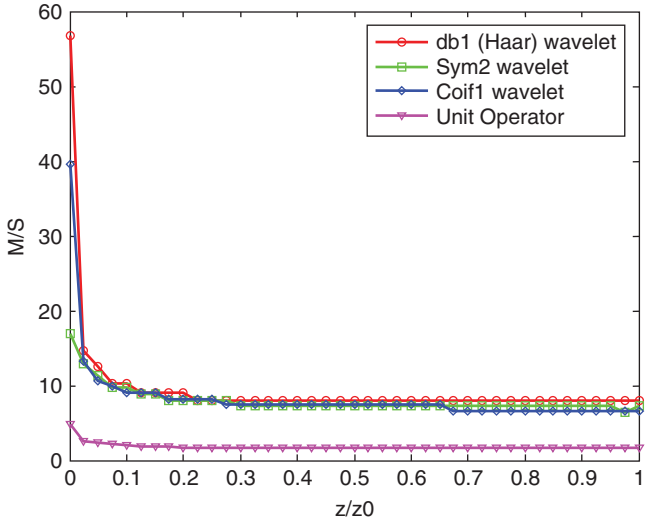

Figure 4.6 (Plate 6) Simulation results showing the normalized compressive sampling ratio for different sparsifying bases [26]. *Source*: Y. Rivenson, A. Stern, and B. Javidi 2013. Reproduced with permission from The Optical Society. *See plate section for the color version*

between the Fresnel transform and the sparsifying operator. Unfortunately, deriving analytical results such as those in Eqs (4.13) and (4.15) for other sparsifying operators, can be extremely tedious. However, we shall demonstrate empirically that the trend of the analysis shown in [11], and predicted by Eqs. (4.13), (4.15) is valid for other popular sparsifying transforms. In Fig. 4.6 (Plate 6), we show simulation results for the normalized samples number ratio M/S obtained with various sparsifying bases: Haar, Coiflet, and Symlet wavelet expansions, compared with those obtained with the canonical representation $\mathbf{\Psi} = \mathbf{I}$. The object is a 1024×1024 pixel USAF 1951 resolution target. In order to reflect the dependence of the number of required samples, M, on z, the curves in Fig. 4.6 were normalized with respect to the sparsity level, S. This is because S depends on the wavelet type being used. For example, in this simulation the Haar expansion yielded $S/N = 0.017$, the Coiflets expansion yielded $S/N = 0.024$, the Symlet expansion yielded $S/N = 0.025$, while $S/N = 0.21$ for the canonical basis. It is witnessed from Fig. 4.6 that the ratio M/S, obtained with various wavelet sparsifying operators, $\mathbf{\Psi}$, shares the same trend as predicted by Eq. (4.13) for $\mathbf{\Psi} = \mathbf{I}$ [11]; that is, it monotonically decreases with the working distance, z, until it approaches a constant asymptote, as predicted by Eq. (4.13). Figure 4.6 also shows that the lowest M/S ratio is achieved by the canonical sparsifying basis. This is expected from the relation between the Fresnel and Fourier transforms, and the fact that Fourier transform holds minimum coherence with the spikes' basis (see Section 4.2).

4.4 Applications of Compressive Digital Holographic Sensing

In this section, we consider holography based applications that take advantage of the CS paradigm. The applications presented here are versatile and include reconstruction

of holograms captured with sparse pixel arrays, sparse camera positions for incoherent holography, reconstruction of an image through a partially occluding aperture, and object tomography from its recorded hologram. These applications, along with others, demonstrate why digital holography has based itself as a leading sensing modality for optical compressive sensing applications.

4.4.1 Compressive Fresnel Holography by Undersampling the Hologram Plane

In this subsection, the problem we wish to address is how to maintain high reconstruction accuracy of the scene while substantially reducing the number of detector pixels. These properties may be useful for reducing detector costs, scanning effort, reducing the captured data volume, or for extracting more information from a measurement. This may be of particular importance for holography in various spectral regimes (e.g., UV, IR, and THz), for incoherent holography or for improving imaging performance.

4.4.1.1 Improved Reconstruction using a Variable Density Subsampling Scheme

A more sophisticated approach can be applied when considering the subsampling scheme in light of the spatial distribution of the sparse coefficients obtained according to the optical setup, and not to just uniformly placing detectors at random across the sampling plane as prescribed by the conventional CS theory. In [9], it was shown that better reconstruction results are achieved when the sampling process puts more emphasis on sampling near the origin of the recorded Fresnel hologram, and less emphasis as we move away from the origin, according to some (non-uniform) probability density function [36].

In Fig. 4.7 we demonstrate this principle by applying a variable density subsampling to an off-axis Fresnel hologram. The object is a 2NIS coin recorded hologram with 100% of the pixels and is shown in Fig. 4.7(a). In Fig. 4.7(b) we see the reconstruction of the +1 order from standard Fresnel back propagation, from the full hologram. Subsampling using the proposed variable density of the full hologram is shown in Fig. 4.7(c), where only 6% of the hologram pixels were selected. This corresponds to only 6% of the measurements. In Fig. 4.7(d) the standard Fresnel back propagation from the subsampled hologram of Fig. 4.7(c) is shown. Due to the subsampling of data the reconstruction in Fig. 4.7(d) is much poorer than in Fig. 4.7(b). However, by applying the CS and reconstruction algorithm the image in Fig. 4.7(e) is obtained, which is almost similar to that obtained with the standard back propagation from full data.

4.4.1.2 Reducing the Scanning Effort in Multiple View Point Projection Incoherent Holography

Compressive digital holographic sensing was also demonstrated to dramatically improve the performance of multiple view projection (MVP) incoherent holography [37]. Multiple view projection holography is a method to obtain a digital hologram using a simple optical setup operating under spatially and temporarily "white" light illuminating conditions. The method requires only a conventional digital camera as a recording device. The MVP method

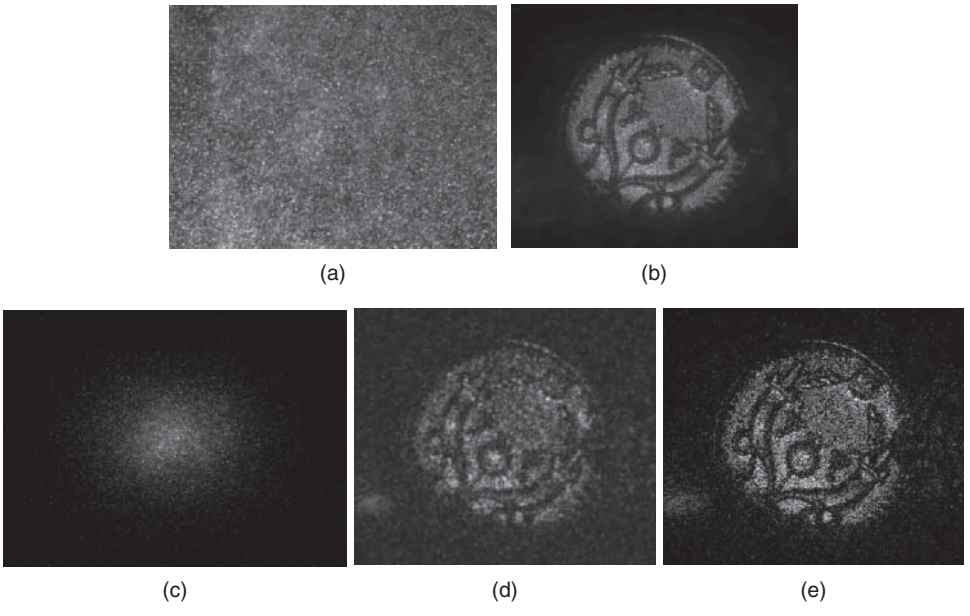

Figure 4.7 CDHS for a reflection, single shot, off-axis hologram. (a) Fresnel hologram of a 2NIS coin. (b) Back propagation reconstruction from the fully sampled hologram in (a). (c) 6% variable density random subsampling of (a). (d) Back propagation reconstruction from (c). Compressive sensing reconstruction in (e) yielding 31.2 dB PSNR (for the region of interest)

is basically divided into two steps as illustrated in Fig. 4.8. The first one is a scene acquisition step, in which multiple views of the scene are acquired by a camera translation. This step usually involves a tedious scanning effort, because it requires a separate camera exposure for each hologram pixel generation [37]. For instance, in order to record a hologram suitable for high definition display, $600 \times 800 \approx 2.88 \times 10^5$ projections should be acquired. The second step is referred to as the digital stage, where each view is digitally multiplied by a corresponding phase functions, and added afterwards. This process ultimately yields a digital Fourier or Fresnel hologram [37].

It was shown in [18] that by adopting the compressive digital holographic sensing approach to MVP holography, a significant reduction of the scanning effort in the acquisition step is possible. This is because (as discussed in Section 4.2), it requires about only $M = S\log N$ hologram pixels in order to accurately reconstruct the scene. Therefore, only $M = S\log N$ different views in the MVP method need to be acquired, instead of N views. Hence, an accurate reconstruction of the 3D scene can be obtained with only a fraction of the nominal number of exposures. The procedure works as follows:

1. Acquire *O(SlogN)* projections of the 3D scene, instead of N projections required for the original MVP algorithm.

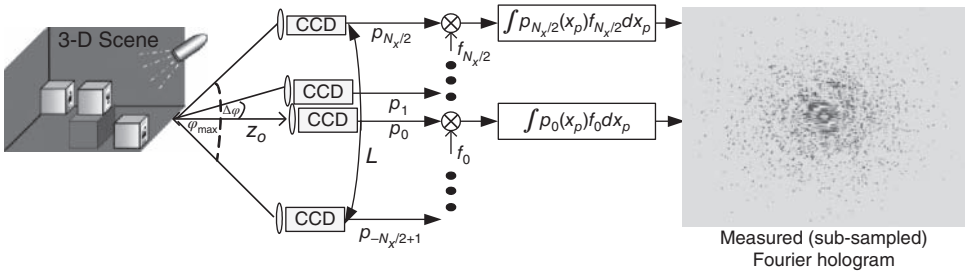

Figure 4.8 An illustration of compressive multiple view projection incoherent holography [18,37]. Using a CCD camera located at distance z_0 from a scene, $K\log N$ projections (denoted by p_i) are captured. Each acquired projection is digitally multiplied and summarized by a corresponding complex function to generate a subsampled hologram. *Source*: Y. Rivenson, A. Stern, and J. Rosen 2011 and N. T. Shaked, B. Katz, and J. Rosen 2009. Reproduced with permission from The Optical Society

2. Multiply each acquired projection by the corresponding phase function, as described previously. This way, a partial Fourier hologram is created, with only a fraction of the projection (coefficients).
3. Reconstruct the signal using the total variation (TV) minimization constraint (4.5). The 3D scene, is reconstructed with focusing on the different planes.

Figure 4.9 (Plate 7) demonstrates simulation results of compressive MVP holography. The simulation was carried as follows: a 3D scene was synthesized where the letters B,G,U were placed at different axial and transversal locations. Each acquired projection was multiplied with a phase function f_n, and then summed, as shown in Fig. 4.8. This way, we have generated a Fourier hologram. The hologram we created was of size 256×256 pixels, which corresponds to 256×256 projections. We than subsampled our resultant Fourier hologram according to the sampling scheme described in Fig. 4.8. For a real experiment, there is no need to acquire all the projections and then subsample; instead one can simply acquire a fraction of the projections needed to reconstruct the scene. The 100% samples were generated in this simulation in order to get a reference for our results. At the next stage a TV (4.5) or (ℓ_1) minimization (4.4) is performed. Figure 4.9 depicts simulation results for different number of compressive samples and different B,G,U letter displacements. No evident difference is found for compressive sensing based reconstruction from 6% of the samples (Figs. 4.9b and e) compared with reconstruction from the fully acquired hologram (Figs. 4.9a and d). The reconstruction results from the compressive sensing when using only 2.5% of the samples is quite satisfactory as well. Other, including real experimental results can be found in [18].

The proposed compressive digital holographic sensing approach for MVP holography holds a number of advantages: First, the acquisition effort is substantially reduced. For instance, if the projections are captured by a scanning process, then the total scanning time may be reduced in order of 15–20 (15–20 times faster). Secondly, less data needs to be transmitted or stored in comparison with conventional MVP methods. The method does not require any additional hardware at the sensor level, and can remedy a temporal object's resolution limitations and bandwidth bottlenecks.

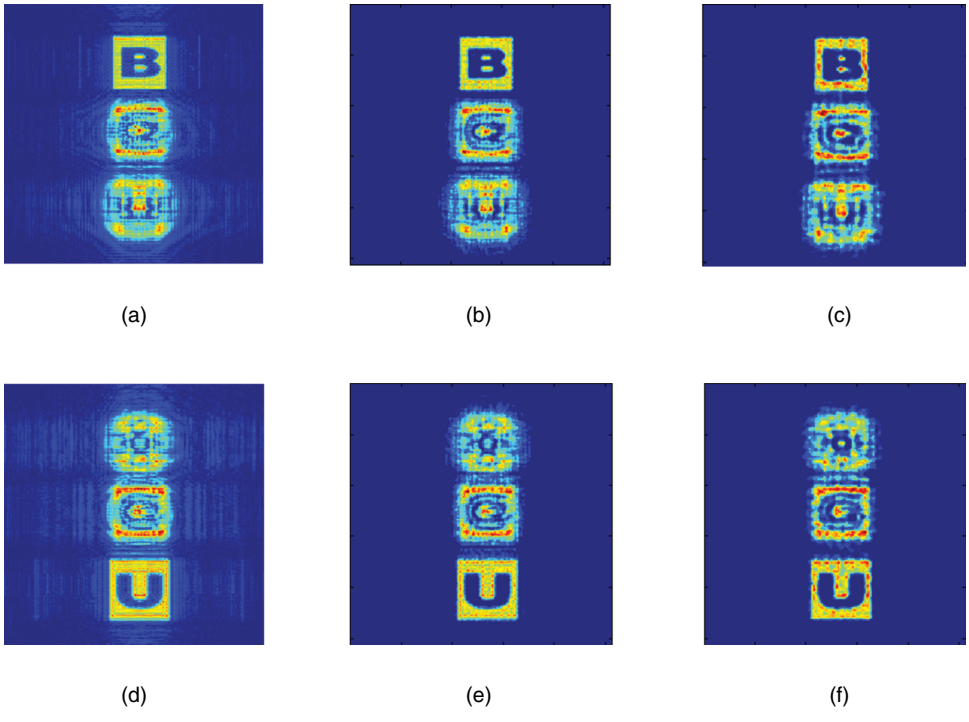

Figure 4.9 (Plate 7) Reconstruction examples of the B (forward) and U (backward) planes. (a) Reconstruction of the B plane form 100% of the projections. (b) CS reconstruction of the B plane forms 6% of the projections. (c) CS reconstruction of the B plane forms 2.5% of the projections. (d) Reconstruction of the U plane forms 100% of the projections. (e) CS reconstruction of the U plane forms 6% of the projections. (f) CS reconstruction of the U plane forms 2.5% of the projections. *See plate section for the color version*

4.4.1.3 Other Applications Applying Compressive Fresnel Holography

The framework of compressive Fresnel holography can also be applied in order to extract super resolved information. This was demonstrated in work by Coskun *et al*. in [15], where the in-line holography framework was used to extract superresolved fluroscence beads and by Liu *et al*. [22], where a compressive digital holograhphy in-line setup was used in order to localize a moving object at an accuracy of (1/45)th of the detector's pixel size.

Another interesting effort is towards the reconstruction of multi-dimensional images as proposed in [21]. Owing CS, only a fraction of the pixels needs to be captured, therefore one can create a sensor in which a small number of pixels capture different information about the object, for example, polarization, color, and so on. Hence it is possible to reconstruct multi-dimensional data with a single shot and without the need of detection hardware for each dimension.

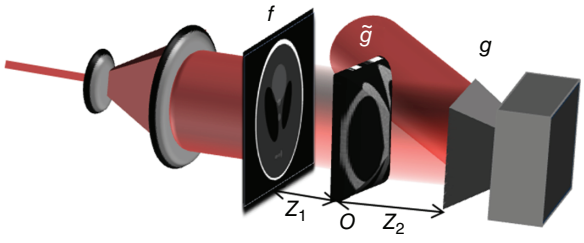

Figure 4.10 A schematic setup for the acquisition of a partially occluded object field. In the object and occluded planes, black represents totally opaque regions, the gray level represents turbid regions

4.4.2 Compressive Digital Holography for Reconstruction of an Object Set Behind an Opaque Medium

Here we show the application of compressive Fresnel holography reconstruction for an object that is set behind a partially opaque media. The sensing mechanism is based on the Fresnel transform of the object. The approach is briefly described in the following paragraphs.

4.4.2.1 Partially Occluded Object Recovery as a Compressive Sensing Problem

The schematic optical setup is shown in Fig. 4.10. Let us assume that the input object $f(x,y)$ is illuminated with a coherent plane wave of wavelength λ. The object's wavefront propagates a distance z_1 and hits a partially occluding plane, $o(x,y)$. The truncated and distorted wavefront propagates another distance, z_2, until it reaches the CCD sensor. This wavefront can be recorded using any of the various holographic techniques.

The occluded object wavefront can be described as follows:

$$g(x,y) = \left[f(x,y) * \exp\left\{ \frac{j\pi}{\lambda z_1} \left(x^2 + y^2\right) \right\} \right] \times o(x,y) * \exp\left\{ \frac{j\pi}{\lambda z_2} \left(x^2 + y^2\right) \right\}. \tag{4.25}$$

It is noted that essentially no information is added or discarded with the free space propagation from the occluding plane to the detector plane; therefore, the information loss is from f(x,y) to $\widetilde{g}(x_{z1}, y_{z1})$. After discretization and applying the numerical far field Fresnel approximation given in Eq. (4.12), together with standard numerical Fresnel back propagation for distance $-z_2$, we obtain:

$$\widetilde{g}(p\Delta x_{z1}, q\Delta y_{z1}) = o(p\Delta x_{z1}, q\Delta y_{z1}) \times \exp\left\{ \frac{j\pi}{\lambda z} \left(p^2 \Delta x_{z1}^2 + q^2 \Delta y_{z1}^2\right) \right\}$$
$$\times \mathcal{F}_{2D}\left[f\left(k\Delta x_0, l\Delta y_0\right) \exp\left\{ \frac{j\pi}{\lambda z_1} \left(k^2 \Delta x_0^2 + l^2 \Delta y_0^2\right) \right\} \right], \tag{4.26}$$

where $0 \le p, q, k, l \le N-1$. The forward sensing model in Eq. (4.26) can be described as a subsampling or distortion (given by the fact that o is not a clear aperture) of the object's Fresnel wave propagation. In this sense it resembles the CS scheme. However, unlike conventional

CS, real world occluding environments are most likely to preserve some sort of structure and certainly cannot be modeled as randomly drawn samples from a uniform distribution.

4.4.2.2 Object Recovery Performance Guarantees

Examining Eq. (4.26) suggests that our ability to accurately reconstruct the object should be determined by μ_2 and Eq. (4.9). For the numerical far field approximation, it can be shown [20] that the coherence parameter μ_2 is given by:

$$\mu_2^{FF} = \max_{m \neq l} \frac{|\widehat{O}(m-l) \otimes \widehat{O}(m-l)|}{\|o\|_2^2}, \tag{4.27}$$

where $\otimes$ denotes the correlation operator, $\|.\|_2$ is the ℓ_2-norm operator and $\widehat{O}$ is the two dimensional Fourier transform of o, $\widehat{O} = \mathcal{F}_{2D}\{o\}$. The indices $0 \leq m, l \leq N-1$ denote the sensing matrix columns. Equation (4.27) holds for the common case where $\Delta x_{z1} = \lambda z_1/(\sqrt{N}\Delta x_0)$ [1,34], while for the more general formulation the reader is referred to [20].

The result in Eq. (4.27) formulates the coherence parameter dependence on the structural properties of the occluding plane. The number of S-sparse signal elements that can be accurately recovered is inversely proportional to μ_2, according to Eq. (4.9).

4.4.2.3 Simulation – Reconstruction of an Object Through a Turbid, Partially Opaque Medium

In the following we illustrate the effectiveness of the method using a simulation. Real experimental results may be found in [20]. The proposed method is demonstrated using a MATLAB simulation. The schematic optical description is shown in Fig. 4.10.

The object in Fig. 4.11(a) is a 512×512 pixel phantom image. A hologram recording process is simulated, according to Eq. (4.26), where an occluding plane shown in Fig. 4.11(b) is composed from totally opaque regions denoted in black and non-opaque regions, which are composed from a complex random media. The non-opaque regions cover merely 28% from the field of view, thus almost three-quarters of the field is blocked. Noise is added at the detector, such that the hologram's SNR is 30 dB. Reconstruction from a noisy hologram of the occluded object using numerical back propagation is shown in Fig. 4.11(c). It can be seen that due to the occlusion most of the object's features are lost. In contrast, an almost perfect reconstruction is shown in Fig. 4.11(d) where the reconstruction is carried out by the proposed formulation of the problem as a compressive Fresnel holography problem.

Thus, we have shown that by using a compressive sensing formulation scheme for holographic imaging of objects located behind a complex partially occluding media an almost exact recovery is possible. This can be achieved using a single shot with an off-axis holography setup or a small number of acquisitions using a phase-shifting holography procedure. The results may be applicable to partially opaque, turbid, or non-linear media, where its physical properties are known in advance, or can be extracted during the object sensing process [20].

4.4.3 Reconstruction of 3D Tomograms from a 2D Hologram

Here we discuss the reconstruction of a 3D object tomography from its single recorded 2D hologram. Numerical reconstruction obtained by digitally focusing on different object depth

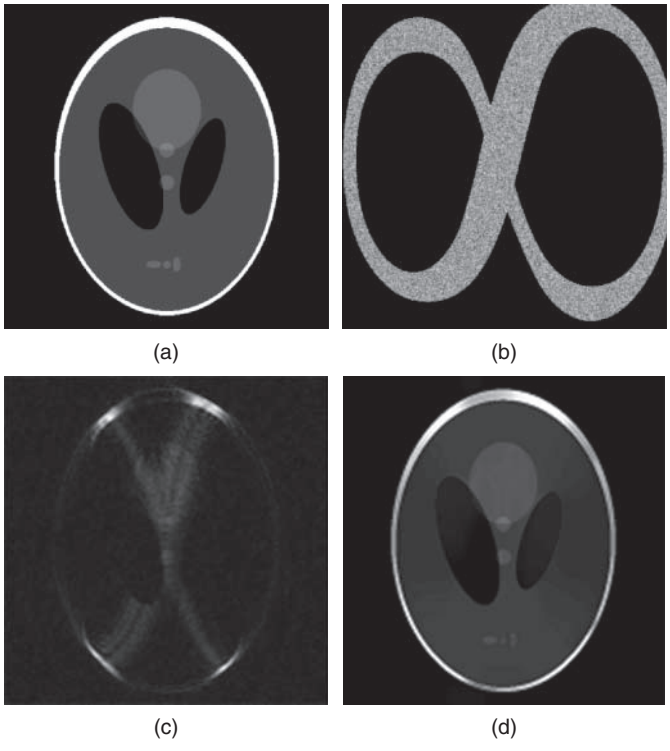

Figure 4.11 Simulation results for phantom reconstruction for an occluded phantom, with added detector noise (SNR of 30dB). (a) Original object (b) Occluding plane, which is composed from complex random areas (grayscale regions) and totally opaque (black regions). (c) Back propagation from the acquired hologram. (d) Reconstruction carried out using the proposed compressive Fresnel holography approach. The resultant reconstruction PSNR = 24.54 dB

planes may be distorted due to out-of-focus object points located in other object planes, as seen in Fig. 4.9. These disturbances are the result of an incomplete model of the system because the back propagation model of Eqs. (4.11)–(4.12) represents a 2D-2D model linking the hologram plane to a single depth plane, thus ignoring other object planes. Clearly, applying reconstruction techniques based on 2D-2D models for 3D-2D acquisition systems is subject to distortions at object points disobeying the model; that is, object points located in another depth planes.

4.4.3.1 Recasting the 3D Object Reconstruction from a Single 2D Hologram as a Compressive Sensing Problem

In order to avoid the out of focus distortions, a 3D-2D forward model relating all the $N_{object} = N_x \times N_y \times N_z$ voxels to $N_{holo} = N_x \times N_y$ hologram pixels should be used. We may formulate

mathematically the (discrete) forward model relating the 3D object, *O(.)*, to its 2D wavefront recorded with the holography process, *U(.)*, as follows:

$$U(k\Delta x, l\Delta y) = \sum_{r=1}^{Nz} \mathcal{F}_{2D}^{-1}\{\mathrm{e}^{-j\pi\lambda r\Delta z[(\Delta v_x m)^2+(\Delta v_y n)^2]}\mathrm{e}^{-j\frac{2\pi}{\lambda}r\Delta z} \times \mathcal{F}_{2D}[f(p\Delta x, q\Delta y; r\Delta z)]\}, \quad (4.28)$$

with $0 \leq p, m \leq N_x - 1$, $0 \leq q, n \leq N_y - 1$, and $1 \leq r \leq N_z - 1$. In Eq. (4.28) the 3D object space is partitioned in a grid with $N_x \times N_y \times N_z$ voxels, each of size $\Delta x \times \Delta y \times \Delta z$. The $\mathcal{F}_{2D}$ operator denotes the 2D discrete Fourier transform. The numerical model in Eq. (4.28) is based on the near field Fresnel approximation but other models may also be considered as discussed in Section 4.3.1. The spatial frequency variables are $\Delta v_x = 1/(N_x\Delta x)$ and $\Delta v_y = 1/(N_y\Delta y)$. This model assumes regular sampling intervals Δz between the different depth planes. The problem of reconstructing the 3D object from its 2D hologram is naturally ill-posed, since there are N_z times more variables than equations. In order to handle this problem we assume that the object is sparse, such that $S < N_{holo}$, therefore we may recast it as a compressive sensing problem. In case where the object in sparse in space domain, we solve the following minimization problem:

$$\min\{\|\mathbf{U} - \mathbf{\Phi}\mathbf{O}^T\|_2^2 + \tau\|\mathbf{O}\|_1\}. \quad (4.29)$$

In Eq. (4.29) $\mathbf{\Phi}$ is the 3D-2D forward model from Eq. (4.28) written as a matrix-vector multiplication such that the vector $\mathbf{U}$ representing the impinging field is:

$$\mathbf{U} = \left[\mathcal{F}_{2D}^{-1}e^{-j\frac{2\pi}{\lambda}\Delta z}\mathbf{Q}_{\lambda^2\Delta z}\mathcal{F}_{2D};\ \ldots\ ;\mathcal{F}_{2D}^{-1}e^{-j\frac{2\pi}{\lambda}N_z\Delta z}\mathbf{Q}_{\lambda^2 N_z\Delta z}\mathcal{F}_{2D}\right][\mathbf{o}_{\Delta z};\ \ldots\ ;\mathbf{o}_{N_Z\Delta z}]^T = \mathbf{\Phi}\mathbf{O}^T, \quad (4.30)$$

where the matrix $\mathbf{Q}_{\lambda^2 r\Delta z}$ is a diagonal matrix which accounts for the quadratic phase terms of Eq. (4.28) and $[\mathbf{o}_{\Delta z};\ \ldots\ ;\mathbf{o}_{N_Z\Delta z}]^T$ is a lexicographical representation of the 3D object. In this case, the reconstruction guarantees for the accurate 3D object from its 2D holographic projection is given by [38]:

$$\mu_2 = \frac{\Delta x\Delta y}{\lambda\Delta z}. \quad (4.31)$$

Thus, by combining Eqs (4.31) and (4.9) we obtain the number of sparse object features that can be accurately reconstructed:

$$S \leq 0.5[1 + \lambda\Delta z/(\Delta x\Delta y)], \quad (4.32)$$

It can be shown that under certain conditions Eq. (4.32) implies axial super-resolution 3D object reconstruction. For more information the reader is referred to [38].

The most widely used tomographic 3D object reconstruction considers the solution of the following TV-norm minimization problem:

$$\min\{\|\mathbf{U} - \mathbf{\Phi}\mathbf{O}^T\|_2^2 + \tau\|\mathbf{O}\|_{TV}\}, \quad (4.33)$$

which is the unconstraint formulation of Eq. (5), where $\|\|_{TV}$ is the 3D total variation operator given by:

$$\|\mathbf{O}\|_{TV} = \sum_l \sum_{i,j} \sqrt{(\mathbf{o}_{i+1,j,l} - \mathbf{o}_{i,j,l})^2 + (\mathbf{o}_{i,j+1,l} - \mathbf{o}_{i,j,l})^2}, \quad (4.34)$$

and τ is a regularization parameter that controls the ratio between the fidelity term and the sparsity level of the object.

This reconstruction approach using the 3D-2D forward model was successfully applied to reconstruction of a 3D object from a single recorded Gabor hologram [8], for reconstruction of a 3D object in the THz regime [12], tomographic reconstruction for diffuse objects from multiple off-axis exposures [13], for incoherent optical scanning holography [14], and also for video rate tomographic microscopy [19]. Recently it was shown that by changing the optical setup and recording the holographic projections of the object from different angles, using the same principles from classic tomography, it is possible to improve reconstruction accuracy [23,24] when combined with the compressive holography technique.

4.4.3.2 Improved Depth Resolution with the Multiple Projection Holography Technique

Here we discuss two other applications of this method. The first is using it for the MVP hologram reconstruction that we have presented in Subsection 4.4.1.2. Like other holography, object reconstruction using the 3D-2D reconstruction model also gives us the ability to improve the tomographic sectioning of the scene; that is, while still taking only a fraction of the projections as explained in Subsection 4.4.1.2. Demonstration of tomographic sectioning of a scene with white light illumination and standard cameras has been shown in [18].

Another benefit from using the compressive holography framework for the MVP generated hologram is described by the following: In multiple aperture systems, the axial resolution increases linearly with the extension of the system's baseline typically defined by its synthetic aperture. This means that the resolution of MVP is linearly proportional to the number of acquired views. However, as shown in [18], when using the compressive digital holographic sensing scheme the axial resolution increases at a higher rate than the required number of projections, by a ratio of $N/S \log N$. This stems from the rule of thumb, which predicts that as the amount of pixels in an image grows, its sparsity level increases at a slower rate. Therefore, the term N/S increases as the dimensionality of the problem increases, and in turn, the ratio of the axial resolution gain relative to the number of projections grows accordingly. Hence, it is possible to obtain the superior axial resolution benefits of the MVP method while reducing the scanning effort. In Fig. 4.12, we illustrate the benefits of CS applied to multiple view projection holography using the following numerical experiment: A synthetic object composed from the letters CDHS was generated where the letters DH were placed at one plane and the letters CS were placed in a more distant plane. A multiple view projection hologram was recorded using only 3275 projections (a representative projection is shown in Fig. 4.12a), which form just about 5% of the nominal number of the 256×256 projections required in the multiple view projection holography method. The obtained hologram is illustrated in Fig. 4.12(b). For contrast, reconstruction using standard numerical back propagation from the subsampled hologram is shown in Fig. 4.12(c). While the reconstruction in Fig. 4.12(c) suffers from severe out-of-plane crosstalk noise, the reconstruction in Fig. 4.12(b) exhibits clear depth slicing.

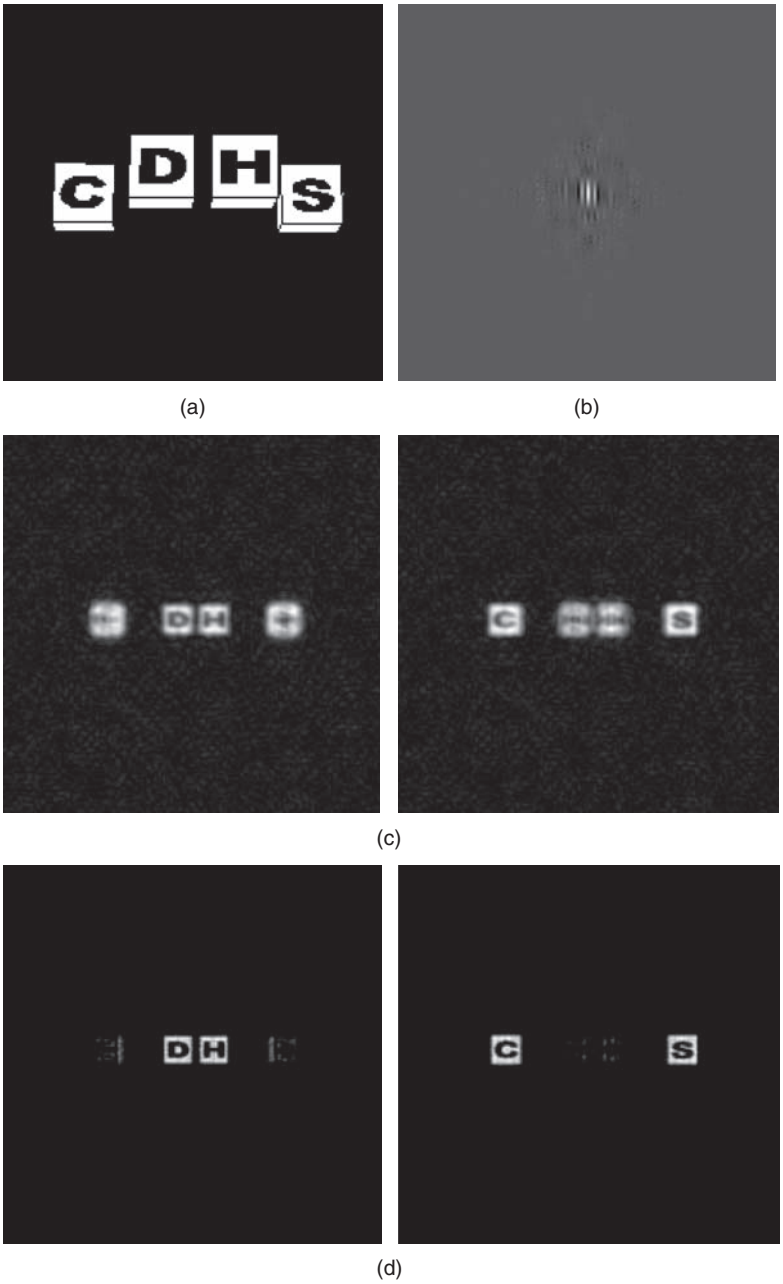

Figure 4.12 Compressive digital holographic sensing (CDHS) applied to multiple view projection incoherent holography. (a) One of the captured views of the scene. (b) Acquired, subsampled hologram, where only 5% of the nominal number views are acquired. (c) Standard numerical back propagation of two of the object planes from (b). (d) The two corresponding planes from (c) reconstructed using the compressive sensing approach. The depth sectioning is evident [26]. *Source*: Y. Rivenson, A. Stern, and B. Javidi 2013. Reproduced with permission from The Optical Society

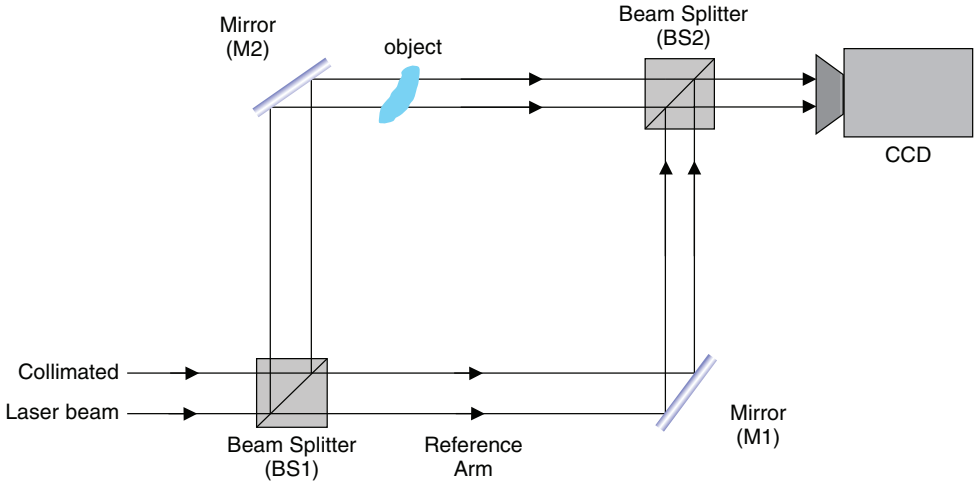

Figure 4.13 A schematic single exposure in line (SEOL) holography setup [26]. *Source*: Y. Rivenson, A. Stern, and B. Javidi 2013. Reproduced with permission from The Optical Society

4.4.3.3 Improved Depth Discrimination using the Single-Exposure In-Line Holography and Compressive Sensing

Another application that was recently demonstrated combined the 3D-2D compressive holography framework with the single exposure in line (SEOL) holography recording setup which was proposed in [39]. The SEOL digital holography was designed for capturing dynamic events in a 3D scene, a micro-organism, or its movement [39–43]. As illustrated in Fig. 4.13, SEOL digital holography utilizes a Mach–Zehnder interferometer setup to record the Fresnel diffraction field of the 3D object in a way similar to phase-shifting digital holography. However, in contrast to phase-shifting on-line digital holography techniques, SEOL digital holography uses only a single exposure. Prior works [39–43] that employed the SEOL holography setup have applied image processing, image recognition, and statistical inference techniques in order to perform tasks such as recognition, tracking, and visualization of micro-organisms. Although it was shown that most interference terms, that is, bias and twin image effects, can often be reduced or neglected in SEOL digital holographic microscopy [42], there are still reconstruction distortions due to out-of-focus object fields located in other object planes, which may impair the analysis tasks.

As explained in Section 4.4.3.1, using the compressive sensing approach with the 3D-2D forward operator leads to improved reconstruction results. This improvement is also apparent when the SEOL recording scheme is employed. Experimental results can be found in [43].

Furthermore, it can be shown that combining the SEOL and compressive holography framework can yield an almost perfect setup for practicing compressive holography. This is owing to three properties of the SEOL. First, the resolution of the system is the same as the in-line holography setup, which is at least twice as high when compared to achievable resolution from an off-axis recording setup. The second property is that for practical microscopic objects, the hologram's acquisition can be performed in a single shot, while allowing satisfactory reconstruction results [41]. The first and second properties are also common for Gabor holography.

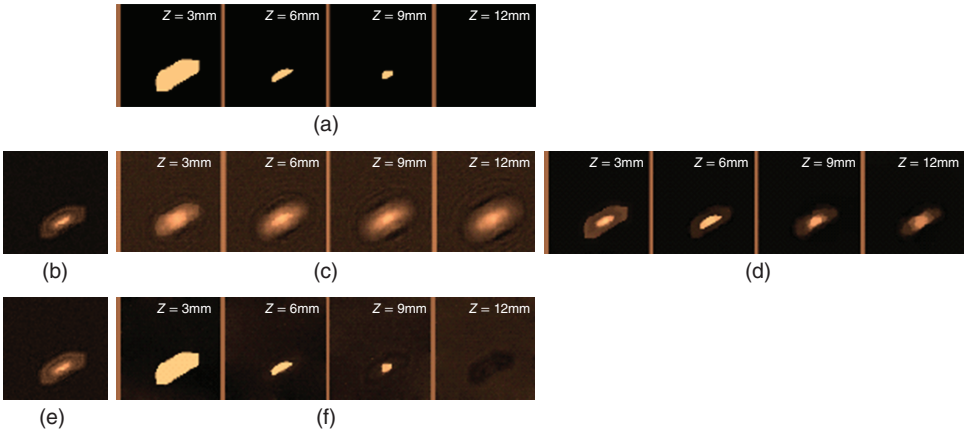

Figure 4.14 (a) Three depth planes of a 3D object. (b) Noisy hologram, (c) depth planes reconstructed using conventional field back-propagation, (d) CS reconstruction results from (b), (e) noisy hologram with reference wave intensity four times larger than in (d), (f) CS reconstructions from (e)

The third property, which differs from Gabor (in-line) holography, is that the SEOL holography behaves as a heterodyne system. This enables the recording of digital holograms with an improved *signal-to-noise ratio* (SNR) by proper control of the amplitude partition of the reference and object arms. The SNR is a figure of merit in DH, and generally its improvement yields enhanced lateral object resolution details [43–45]. Combining this property of the SEOL setup, while introducing the CS formulation, has yielded improved axial resolution with comparison to compressive reconstruction from a Gabor holographic recording [43]. This is demonstrated in Fig. 4.14 where the results of a numerical experiment demonstrates improved axial resolution (3D sectioning) by approaching SEOL in a CS framework together with proper intensity partition on the reference and object beams [43]. In this simulation, the reference beam was set to be four times larger than the object's beam intensity. Comparing the reconstruction results from of the standard back-propagation, compressive holography reconstruction with the hologram recorded in Gabor setup, and compressive SEOL holography reconstruction, it can be witnessed that the latter gives the most accurate reconstruction results.

We may conclude that the SEOL digital holographic setup, combined with the compressive sensing framework can be considered an almost ideal 3D object inference digital holographic based system; it offers the high resolution and large FOV associated with Gabor holography, and provides the robustness and sensitivity associated with off-axis holography setup, along with rapid frame acquisition rate associated with Gabor and off-axis configurations.

4.5 Conclusion

In this chapter we have demonstrated the usefulness of compressive sensing theory in the realm of digital holography. The basic compressive sensing theory was presented along with theoretical analysis of implementation aspects for digital holography. The analysis accounted for the imaging geometry, type of illumination, sensor size and resolution, object spatial size and resolution, sparsity of the object, and sparsifying transform used for representing the object.

A brief survey of compressive digital holographic sensing applications was presented. We have also demonstrated that CS together with appropriate modeling can help in recovering objects imaged through a complex random and/or partially opaque media. Furthermore, inference of an object tomography from its hologram was discussed. Improvement of the 3D resolution with incoherent multiple view projection holography, and with in-line SEOL holography, were demonstrated.

In summary, we have shown that CS can drastically improve the extraction of the information captured with holographic setups. We believe that future mutual synergies between digital holography and compressive sensing will demonstrate further improvements in 3D imaging performance, will yield new optical setup designs, and enable new applications.

Acknowledgments

This work was supported by the Israel Ministry of Science and Technology (MOST) to YR, AS and JR, and by The Israel Science Foundation (ISF) to AS and JR.

References

[1] Kreis T., *Handbook of Holographic Interferometry*, 1st edn, Wiley-VCH Verlag, Weinheim), Chap. 3 (2004).
[2] Donoho D., "Compressed sensing", *IEEE Trans. on Information Theory*, **52**(4), 1289–1306 (2006).
[3] Candès E. J., J. K. Romberg, and T. Tao, "Stable signal recovery from incomplete and inaccurate measurements", *Communications on Pure and Applied Mathematics* **59**(8), 1207–1223 (2006).
[4] Eldar Y. C. and G. Kutyniok, *Compressed Sensing: Theory and Applications*, Cambridge University Press (2012).
[5] Bruckstein A. M., D. L. Donoho, and M. Elad, "From Sparse Solutions of Systems of Equations to Sparse Modeling of Signals and Images", *SIAM Review* **51**(1), 34–81 (2009).
[6] Stern A., "Method and system for compressed imaging", US patent app. Nr. **12**/605866 (2008).
[7] Denis L., D. Lorenz, E. Thiébaut, C. Fournier, and D. Trede, "Inline hologram reconstruction with sparsity constraints," *Opt. Lett.* **34**, 3475–3477 (2009).
[8] Brady D. J., K. Choi, D. L. Marks, R. Horisaki, and S. Lim, "Compressive Holography," *Opt. Express* **17**, 13040–13049 (2009).
[9] Rivenson Y., A. Stern, and B. Javidi, "Compressive Fresnel holography," *Display Technology, Journal of* **6**(10), 506–509 (2010).
[10] Marim M. M., M. Atlan, E. Angelini, and J.-C. Olivo-Marin, "Compressed sensing with off-axis frequency-shifting holography," *Opt. Lett.* **35**, 871–873 (2010).
[11] Rivenson Y. and A. Stern, "Conditions for practicing compressive Fresnel holography," *Opt. Lett*. **36**, 3365–3367 (2011).
[12] Fernandez Cull C., D. A. Wikner, J. N. Mait, M. Mattheiss, and D. J. Brady, "Millimeter-wave compressive holography," *Appl. Opt.* **49**, E67–E82 (2010).
[13] Choi K., R. Horisaki, J. Hahn, S. Lim, D. L. Marks, T. J. Schulz, and D. J. Brady, "Compressive holography of diffuse objects," *Appl. Opt.* **49**, H1–H10 (2010).
[14] Zhang X. and E. Y. Lam, "Edge-preserving sectional image reconstruction in optical scanning holography," *J. Opt. Soc. Am. A* **27**, 1630–1637 (2010).
[15] Coskun A. F., I. Sencan, T.-W. Su, and A. Ozcan, "Lensless wide-field fluorescent imaging on a chip using compressive decoding of sparse objects," *Opt. Express* **18**, 10510–10523 (2010).

[16] Greenbaum A., W. Luo, T. Su, Z. Göröcs, L. Xue, S. O. Isikman, *et al*., Imaging without lenses: Achievements and remaining challenges of wide-field on-chip microscopy. *Nature Methods* **9**(9), pp. 889–895 (2012).
[17] Marim M., E. Angelini, J.-C. Olivo-Marin, and M. Atlan, "Off-axis compressed holographic microscopy in low-light conditions," *Opt. Lett.* **36**, 79–81 (2011).
[18] Rivenson Y., A. Stern, and J. Rosen, "Compressive multiple view projection incoherent holography," *Opt. Express* **19**, 6109–6118 (2011).
[19] Hahn J., S. Lim, K. Choi, R. Horisaki, and D. J. Brady, "Video-rate compressive holographic microscopic tomography," *Opt. Express* **19**, 7289–7298 (2011).
[20] Rivenson Y., A. Rot, S. Balber, A. Stern, and J. Rosen, "Recovery of partially occluded objects by applying compressive Fresnel holography," *Opt. Lett.* **37**, 1757–1759 (2012).
[21] Horisaki R., J. Tanida, A. Stern, and B. Javidi, "Multidimensional imaging using compressive Fresnel holography," *Opt. Lett.* **37**, 2013–2015 (2012).
[22] Liu Y., L. Tian, J. Lee, H. Huang, M. Triantafyllou, and G. Barbastathis, "Scanning-free compressive holography for object localization with subpixel accuracy," *Opt. Lett.* **37**, 3357–3359 (2012).
[23] Nehmetallah G. and P. Banerjee, "Applications of digital and analog holography in three-dimensional imaging," *Adv. Opt. Photon*. **4**, 472–553 (2012).
[24] Williams L., G. Nehmetallah, and P. Banerjee, "Digital tomographic compressive holographic reconstruction of 3D objects in transmissive and reflective geometries," *App. Opt*. **52**, 1702–1710 (2013).
[25] Lim S., D. Marks, and D. Brady, "Sampling and processing for compressive holography," *Appl. Opt.* **50**, H75–H86 (2011).
[26] Rivenson Y., A. Stern, and B. Javidi, "Overview of compressive sensing techniques applied in holography," *Appl. Opt.* **52**, A423–A432 (2013).
[27] Stern A. and B. Javidi, "Random projections imaging with extended space-bandwidth product," *Journal of Display Technology* **3**(3), 315–320 (2007).
[28] Donoho D. L. and M. Elad, "Optimally sparse representation in general (nonorthogonal) dictionaries via ℓ_1 minimization," *Proc. Nat. Acad. Sci. USA*, **100**(5), 2197–2202 (2003).
[29] Candès E. J. and Y. Plan, A probabilistic and RIPless theory of compressed sensing. *IEEE Transactions on Information Theory* **57**(11), 7235–7254 (2011).
[30] Rudin L., S. Osher and E. Fatemi, "Nonlinear total variation based noise removal algorithm," *Physica D* **60**, 259–268 (1992).
[31] Needell D. and R. Ward, "Stable image reconstruction using total variation minimization," *SIAM Journal on Imaging Sciences* **6**(2), 1035–1058 (2013).
[32] Lustig M., D. L. Donoho, J. M. Santos and J. M. Pauly, "Compressed Sensing MRI," *IEEE Signal Processing Magazine* **25**(2), 72–82 (2008).
[33] Candès E. J. and J. Romberg, "Sparsity and incoherence in compressive sampling," *Inverse Problems* **23**, 969–985 (2006).
[34] Mas D., J. Garcia, C. Ferreira, L. M. Bernardo and F. Marinho, "Fast algorithms for free-space diffraction patterns calculation," *Opt. Comm.* **164**, 233–245 (1999).
[35] Rivenson Y. and A. Stern, "Compressed imaging with separable sensing operator," *IEEE Signal Processing Letters* **16**(6), 449–452 (2009).
[36] Van der Lught A., "Optimum sampling of Fresnel transforms," *Applied Optics* **29**, 3352–3361 (1990).
[37] Shaked N. T., B. Katz, and J. Rosen, "Review of three-dimensional holographic imaging by multiple-viewpoint-projection based methods," *Appl. Opt.* **48**, H120–H136 (2009).
[38] Rivenson Y., A. Stern, and J. Rosen, "Reconstruction guarantees for compressive tomographic holography," *Opt. Lett.* **38**, 2509–2511 (2013).
[39] Javidi B., I. Moon, S. Yeom and E. Carapezza, "Three-dimensional imaging and recognition of microorganism using single-exposure on-line (SEOL) digital holography," *Opt. Express* **13**, 4402–4506 (2005).

[40] Yeom S. and B. Javidi, "Automatic identification of biological microorganisms using three-dimensional complex morphology," *J. Biomed. Opt*. **11**, 024017 (2006).
[41] Stern A. and B. Javidi, "Theoretical analysis of three-dimensional imaging and recognition of micro-organisms with a single-exposure on-line holographic microscope," *J. Opt. Soc. Am. A* **24**, 163–168 (2007).
[42] Moon I., M. Daneshpanah, B. Javidi, and A. Stern, "Automated three-dimensional imaging, identification and tracking of micro/nano biological organisms by holographic microscopy," *Proc. IEEE* **97**, 990–1010 (2009).
[43] Rivenson Y., A. Stern, and B. Javidi, "Improved three-dimensional resolution by single exposure in-line compressive holography," *Appl. Opt.* **52**, A223–A231 (2013).
[44] Charrière F., T. Colomb, F. Montfort, E. Cuche, P. Marquet, and C. Depeursinge, "Shot-noise influence on the reconstructed phase image signal-to-noise ratio in digital holographic microscopy," *Appl. Opt.* **45**, 7667–7673 (2006).
[45] Tippie A. and J. Fienup, "Weak-object image reconstructions with single-shot digital holography," in *Digital Holography and Three-Dimensional Imaging*, OSA Technical Digest (Optical Society of America, 2012), paper DM4C.5.